

文章编号: 1001-3555(2022)02-0162-09

CO₂ 加氢制甲酸理论研究及高效铁基催化剂设计

刘 聪¹, 胡兴邦^{2*}

(1. 山东国邦药业股份有限公司, 山东潍坊 261108; 2. 南京大学 化学化工学院, 江苏南京 210023)

摘要: CO₂加氢制甲酸由于需同时活化惰性氢气及CO₂而富有挑战性, 同时此过程原子经济性100%, 具有很好的理论和现实研究价值, 但文献中报道的活性较好的催化剂均为贵金属催化剂。为了开发活性更高的用于CO₂加氢制甲酸的铁基催化剂, 我们采用理论计算方法研究了12种不同种类的PNP-Fe(PNP=2,6-(二-叔丁基-磷甲基)吡啶)化合物催化CO₂加氢制甲酸的过程。理论研究结果表明, CO₂加氢制甲酸反应过程包括H₂活化及CO₂插入金属氢键两个步骤, H₂活化过程是整个反应的速控步骤。催化剂吡啶环上进行P原子取代可以显著降低H₂活化能垒。基于以上发现, 我们设计了一种新颖的高效铁基催化剂, 使用此催化剂催化CO₂加氢制甲酸反应, 速控步骤能垒只有85.6 kJ/mol, 催化活性与贵金属的比较接近。我们研究的12种铁基催化剂速控步骤能垒范围为85.6~126.4 kJ/mol, 显示了配体良好的调控催化活性能力。

关键词: CO₂; 加氢; 甲酸; 理论计算; 铁基催化剂

中图分类号: O621.1

文献标志码: A

DOI: 10.16084/j.issn1001-3555.2022.02.007

二氧化碳(CO₂)是一种主要温室气体。近年来, 大气中的CO₂浓度正快速增加。为此, 我国明确提出了“碳达峰”和“碳中和”目标。使用CO₂为原料合成有用的化工产品是碳减排的有效途径。越来越多的学术和产业界研究人员开始关注CO₂的利用问题^[1]。

在文献报道的CO₂利用方法中, CO₂加氢制甲酸是最吸引人的过程之一^[2-4]。一方面, 甲酸在工业上被广泛使用。另一方面, CO₂加氢制甲酸具有100%的原子经济性。CO₂加氢包括两个步骤: 氢气(H₂)活化形成金属-氢(M-H)键以及CO₂插入M-H键^[3-16]。这一反应由于需同时活化惰性的CO₂和H₂而充满挑战。开发高活性催化剂对于实现CO₂加氢制甲酸极为重要。文献中报道的CO₂加氢制甲酸催化剂包括贵金属(如Ir^[17-18]、Rh^[19-20]、Ru^[21-22]、Pt^[23]、Pd^[24-25]和Re^[26])和非贵金属(如Cu^[27-28]、Mn^[29-30]、Fe^[31-34]、Co^[35-36]和Mo^[37])催化剂。在这些催化剂中, 贵金属催化剂展现出了很高的催化活性, 而非贵金属催化剂活性较低。比如, 基于Ir的^{tBu}PNP-Ir(III)催化剂的每摩尔催化剂单位活性中心上底物的转化数(TON)高达3 500 000^[17]。同样, 基于Ru的^{tBu}PNP-Ru催化剂的TON达到

6 000 000^[21]。相对而言, 非贵金属催化剂的活性要低很多。基于Co的Co(dmpe)₂H代表了活性最高的CO₂加氢制甲酸非贵金属催化剂, 但其TON只有9400^[35], 比^{tBu}PNP-Ir(III)和^{tBu}PNP-Ru的TON分别低了372^[17]和638^[21]倍。

尽管贵金属催化剂的催化活性非常优异, 但昂贵的价格严重限制了其大规模工业化应用。铁(Fe)是地球上含量最丰富的过度金属元素之一。然而, 文献报道的CO₂加氢制甲酸铁基催化剂活性都非常低。比如, 基于Fe的PNP-Fe(III)的TON只有788^[31]。

PNP型金属配合物在CO₂加氢制甲酸过程中被广泛使用^[17,19,21,31]。作为课题组在CO₂加氢领域工作的重要组成部分^[28,38-39], 我们对基于Fe的PNP-Fe化合物进行不同官能化修饰理论研究, 期望从理论上揭示能大幅提升PNP-Fe催化CO₂加氢制甲酸活性的方法, 为高效CO₂加氢制甲酸催化剂开发提供理论基础。

1 计算方法

众所周知, 密度泛函理论(DFT)在给出合理计算结果的同时具有较高的计算效率。基于DFT

收稿日期: 2021-01-23; 修回日期: 2022-02-01。

基金项目: 国家自然科学基金面上项目(22178159和21878141)(National Natural Science Foundation of China (No. 22178159 and 21878141))。

作者简介: 刘聪(1979-), 男, 高级工程师(LIU Cong(1979-), male, Senior Engineer)。

* 通讯联系人, E-mail: huxb@nju.edu.cn。

的B3LYP方法已经被广泛用于贵金属和非贵金属催化的CO₂加氢制甲酸反应^[6-7,10,16,38-39],并给出了可与实验相佐证的计算结果^[6,16,38-39]。因此,我们采用Gaussian09程序所包含的B3LYP方法进行计算。对于体系中的金属原子,使用LANL2DZ基组。对于除金属外的其它原子,使用6-311+G*基组(后文简写为B3LYP/LANL2DZ/6-311+G*)。计算中使用EmpiricalDispersion=GD3BJ关键词进行色散校正。所有的结构优化、能量计算以及零点能校正都采用以上所述计算方法。计算所得过渡态均有且只有一个虚频。由于CO₂加氢制甲酸常常在四氢呋喃中进行^[28,38-39],因此我们进一步采用PCM溶剂模型、使用UFF原子半径、以四氢呋喃为溶剂,对所有优化构型进行了能量计算以及零点能校正(溶剂效应修正采用气态优化所得构型)。热力学修正的温度和压力分别是25.15℃和0.10 MPa。

计算同时考虑了过渡金属的高、低两种不同自旋态。对于PNP-M(M=Fe, Ru)而言,低自旋态化合物(自旋多重度=1)远比高自旋态(自旋多重度=3)的要稳定。比如,高自旋态PNP-Ru的吉布斯自由能比低自旋态的要高195.3 kJ/mol。高自旋态PNP1-Fe的吉布斯自由能比低自旋态的要高165.5 kJ/mol。因此,后续主要关注更加稳定的低自旋态PNP-M催化剂及其催化的反应过程。同时,由于催化剂自旋态能量差远高于反应最大活化能能垒高度,因此反应过程不存在自旋交叉。文献中采用Fe或Ru类催化剂催化CO₂加氢制甲酸的理论计算,同样也没有自旋交叉存在^[9,13,16]。

2 结果与讨论

在迄今文献报道的CO₂加氢制甲酸催化剂中,^tBuPNP-Ru具有最高的催化活性(TON=6 000 000^[21])。因此,我们首先对^tBuPNP-Ru催化的CO₂加氢制甲酸过程进行研究,相应活化能数据可以作为标准来评估进一步设计的PNP-Fe催化剂活性。结合文献对CO₂加氢制甲酸的理论计算结果^[3-16],我们采用图1所示催化循环机制:首先CO₂插入M-H键形成M-HCO₂中间体(Int1),然后Int1上的HCO₂阴离子旋转形成更加稳定的M-OCOH中间体(Int2),接下来活化氢气形成催化剂-甲酸配合物(Pro),最后在碱的作用下催化剂得以还原并生成甲酸盐。

图2展示了PNP-Ru催化CO₂加氢制甲酸过程的CO₂插入Ru-H键以及H₂活化形成Ru-H

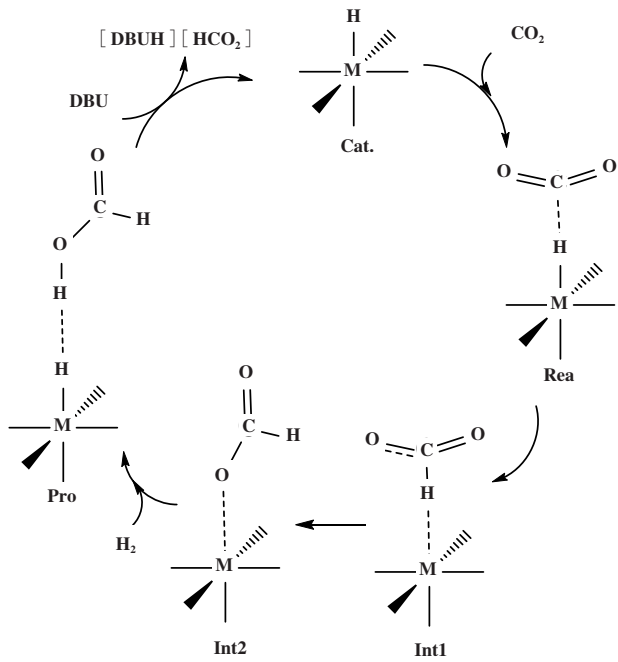


图1 CO₂加氢制甲酸催化循环
(Rea→Int2: CO₂插入; Int2→Pro: H₂活化)
Fig.1 The catalytic process of CO₂ hydrogenation to formic acid
(Rea→Int2: CO₂ insertion; Int2→Pro: H₂ activation)

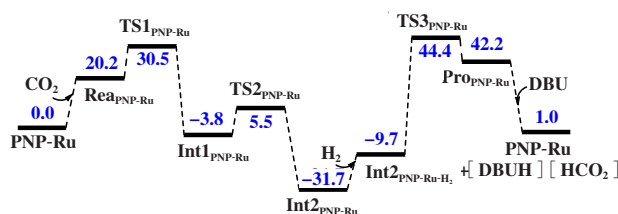


图2 含CO₂、H₂结合过程的PNP-Ru催化的CO₂加氢制甲酸能量图

Fig.2 The energy diagram of CO₂ hydrogenation to formic acid catalyzed by PNP-Ru including the binding processes of CO₂ and H₂(the shown values are Gibbs free energy in kJ/mol, calculation method: B3LYP/LANL2DZ/6-311+G*; energy barrier for CO₂ insertion and H₂ activation are 30.5 and 76.1 kJ/mol respectively)

键等步骤的吉布斯自由能变化。图3展示了PNP-Ru催化的CO₂加氢制甲酸反应物、过渡态、中间体、产物的优化构型。Ru-H键上的氢可经由过渡态TS1_{PNP-Ru}从活性中心Ru向CO₂迁移,相应活化能只有30.5 kJ/mol。之后,形成包含HCO₂基团的中间体Int1_{PNP-Ru}。HCO₂基团可经由TS2_{PNP-Ru}过渡态发生旋转形成中间体PNP-Ru-OCOH(Int2_{PNP-Ru})。紧接着,通过过渡态TS3_{PNP-Ru}对H₂进行活化。H₂与

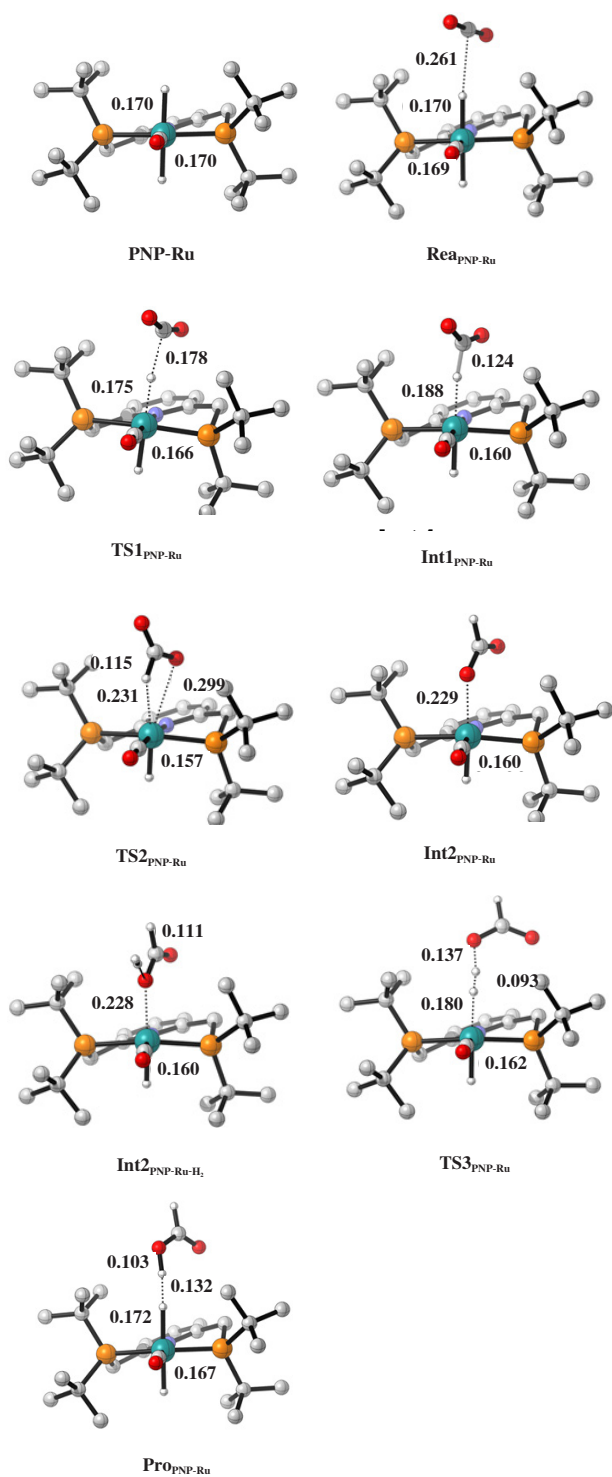


图3 含 CO_2 、 H_2 结合过程的 PNP-Ru 催化的 CO_2 加氢制甲酸反应物、过渡态、中间体、产物的优化构型

Fig.3 The optimized structures of the reactant, transition states, and intermediates in the CO_2 hydrogenation to formic acid catalyzed by PNP-Ru including the binding processes of CO_2 and H_2 (The shown values are bond length in nm, calculation method:

B3LYP/LANL2DZ/6-311+G^{*})

$\text{Int2}_{\text{PNP-Ru}}$ 结合为吸热过程, 过渡态 $\text{TS3}_{\text{PNP-Ru}}$ 中 $\text{H}-\text{H}$ 键长为 0.093 nm, 与 $\text{Rh}(\text{PH}_3)_2$ (0.110 nm)^[3] 和石墨烯负载 Cu (0.101 nm)^[11] 催化的过程十分相似。活化 H_2 的过渡态 $\text{TS3}_{\text{PNP-Ru}}$ 的能垒为 76.1 kJ/mol, 这一较低的能垒使得 PNP-Ru 成为目前实验上观察到活性最高的 CO_2 加氢制甲酸催化剂之一^[21]。

经由 $\text{TS3}_{\text{PNP-Ru}}$ 可以得到 PNP-Ru- 甲酸配合物。研究已经表明 CO_2 加氢制甲酸过程在热力学上不利^[40], 因此往往需额外添加有机或无机碱来推动反应进行^[17-37], 即通过碱使甲酸从催化剂上脱落, 形成甲酸盐, 同时催化剂得以恢复。1,8- 二氮杂双环 [5.4.0]十一碳-7- 烯 (DBU) 是 CO_2 加氢制甲酸常采用的碱, 在 DBU 存在下, 催化循环总的吉布斯自由能变是 1.0 kJ/mol (图 2)。由于吉布斯自由能为微小的正值, 所以文献中常常采用加入过量碱的方法来推动反应进一步进行^[17-37]。

为了研究配体修饰对铁基催化剂催化活性的影响并发现活性更高的 CO_2 加氢制甲酸催化剂, 我们一共研究了 12 种具有不同结构的 Fe 基催化剂(图 4)。这些催化剂包括在 PNP 配体上进行不同吸电、

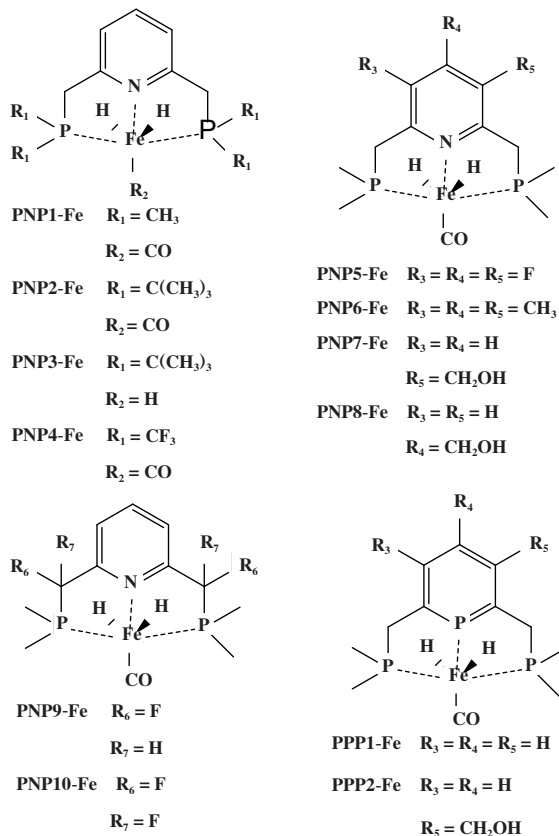


图4 铁基催化剂结构

Fig.4 The structures of Fe-based catalysts

给电修饰的结构(PNP1~PNP6、PNP9 和 PNP10), 包含及不包含分子内氢键的结构(PNP7、PNP8 和 PPP2). 此外, 还将 PNP 配体吡啶环上的 N 原子替换为 P 原子(PPP1 和 PPP2).

图 5 和图 6 展示了 PNP1-Fe 催化 CO₂ 加氢制甲酸过程的 H₂ 活化形成 Fe—H 键以及 CO₂ 插入 Fe—H 键等步骤的能量图及优化构型. Fe—H 键上的氢可经由过渡态 TS1_{PNP1-Fe} 向 CO₂ 移动, 相应过渡态能垒只有 55.2 kJ/mol. H₂ 活化也是 PNP1-Fe 催化过程的速控步骤, 相应过渡态能垒为 99.9 kJ/mol. 这一 H₂ 活化能垒比使用 PNP-Ru 为催化剂时的高出 23.8 kJ/mol, 这使得 PNP1-Fe 具有相对较低活性.

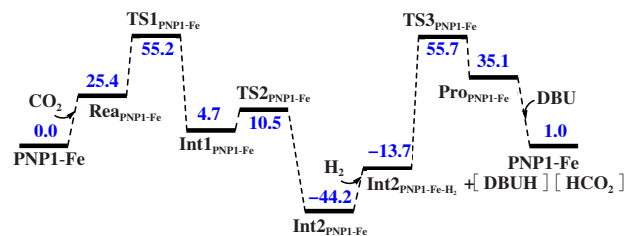


图5 含CO₂、H₂结合过程的PNP1-Fe催化的CO₂加氢制甲酸能量图

Fig.5 The energy diagram of CO₂ hydrogenation to formic acid catalyzed by PNP1-Fe including the binding processes of CO₂ and H₂(The shown values are Gibbs free energy in kJ/mol, calculation method: B3LYP/LANL2DZ/6-311+G^{*}; energy barrier for CO₂ insertion and H₂ activation are 55.2 and 99.9 kJ/mol respectively)

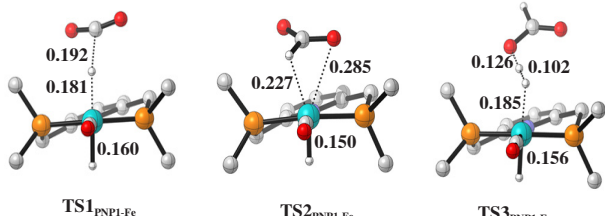


图6 含CO₂、H₂结合过程的PNP1-Fe催化的CO₂加氢制甲酸过渡态的优化构型

Fig.6 The optimized structures of transition states in the CO₂ hydrogenation to formic acid catalyzed by PNP1-Fe including the binding processes of CO₂ and H₂(The shown values are bond length in nm, calculation method: B3LYP/LANL2DZ/6-311+G^{*})

由于 H₂ 活化是 CO₂ 加氢制甲酸过程的速控步骤, 我们还研究了其他修饰方式的 PNP-Fe 催化剂催化 H₂ 的活化过程. 图 7 展示了不同修饰 PNP-Fe

催化 CO₂ 加氢制甲酸过程的 H₂ 活化形成 Fe—H 键

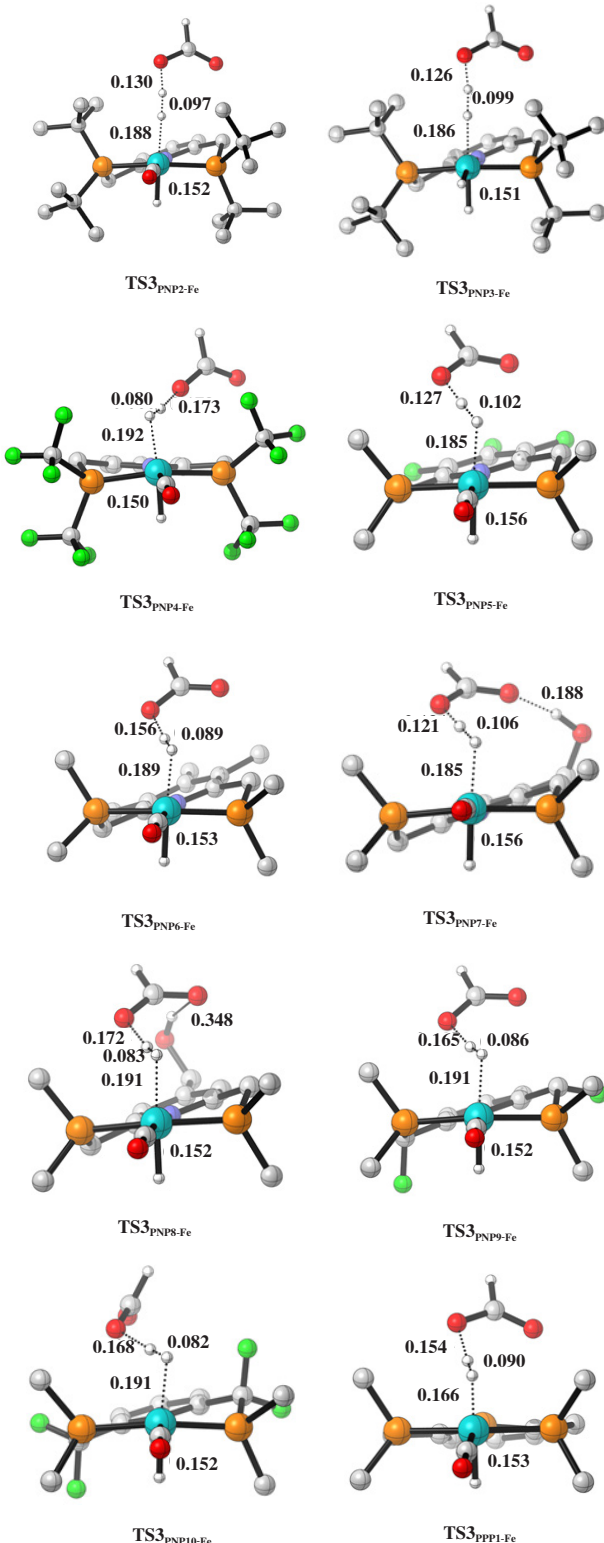


图7 使用不同PNP-Fe催化剂速控步骤过渡态的优化构型

Fig.7 The optimized transition states using different Fe-based catalysts (The values are bond length in nm, calculation method: B3LYP/LANL2DZ/6-311+G^{*})

的过渡态优化构型, 对应的能量展示于表1中。将PNP-Fe上和Fe配位的CO替换为H原子会使H₂

活化能垒增加19.1 kJ/mol (TS3_{PNP2-Fe} vs. TS3_{PNP3-Fe})。在PNP配体上进行F原子修饰也会显著增加H₂活

表1 不同催化剂速控步骤活化能垒

Table 1 The energy barriers of rate-determining step in the presence of different catalysts

Catalysts	Energy barriers/(kJ·mol ⁻¹)	Catalysts	Energy barriers/(kJ·mol ⁻¹)
PNP-Ru	76.1	PNP1-Fe	99.9
PNP2-Fe	88.5	PNP3-Fe	107.6
PNP4-Fe	126.4	PNP5-Fe	109.8
PNP6-Fe	89.5	PNP7-Fe	91.2
PNP8-Fe	96.6	PNP9-Fe	95.4
PNP10-Fe	115.2	PPP1-Fe	85.6
PPP2-Fe	87.6		

化能垒。比如, 将P原子上的-CH₃修饰为-CF₃使H₂活化能垒增加37.9 kJ/mol。将吡啶环上的H原子进行F原子取代后, H₂活化能垒增加了21.3 kJ/mol (TS3_{PNP5-Fe} vs. TS3_{PNP1-Fe})。在亚甲基上进行F原子取代也给出类似的结果(TS3_{PNP9-Fe} 和 TS3_{PNP10-Fe})。在P原子上进行-CH₃取代, 有利于中间体Int2和H₂的结合, 从而使得反应活化能下降, 比如TS3_{PNP2-Fe}的活化能比TS3_{PNP1-Fe}的低47.7 kJ/mol。引入分子内氢键可稳定H₂活化过渡态TS₃, 从而降低过渡态能垒。比如, TS3_{PNP7-Fe}的能垒比TS3_{PNP1-Fe}的要低8.7 kJ/mol。而当分子内氢键比较弱时, 其对降低活化能的贡献也相应变弱(TS3_{PNP7-Fe} 和 TS3_{PNP8-Fe})。值得注意的是, 将PNP配体吡啶环上的N原子替换为P原子能显著降低H₂活化能垒14.3 kJ/mol (TS3_{PPP1-Fe} vs. TS3_{PNP1-Fe})。

基于以上发现, 我们设计了一个包含分子内氢键及P原子取代的催化剂(PPP2-Fe)。希望通过P原子取代来调控活性中心金属Fe的电子结构、同时通过分子内氢键来稳定过渡态, 从而获得更高活性的CO₂加氢制甲酸催化剂。图8展示了PPP2-Fe催化CO₂加氢制甲酸过程的H₂活化形成Fe—H键以及CO₂插入Fe—H键两个步骤的能量图。图9展示了PPP2-Fe催化的CO₂加氢制甲酸反应物、过渡态、中间体、产物的优化构型。非常值得注意的是, 使用PPP2-Fe进行H₂活化, 相应活化能垒为87.6 kJ/mol, 比不含氢键的PPP1-Fe体系的能垒稍高2.0 kJ/mol。虽然氢键形成可在一定程度上稳定过渡态, 通过对TS3_{PPP2-Fe}和TS3_{PPP1-Fe}的结构可以发现, 对于

P取代的催化体系而言, 氢键形成过程会引起芳环结构一定扭曲, 从而抵消了氢键的稳定贡献。当使

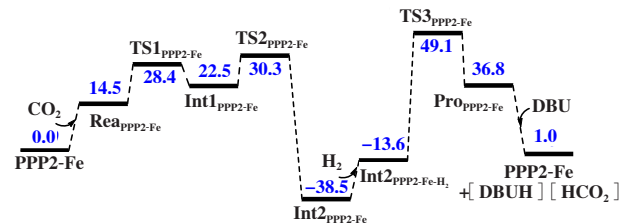


图8 含CO₂、H₂结合过程的PPP2-Fe催化的CO₂加氢制甲酸能量图

Fig.8 The energy diagram of CO₂ hydrogenation to formic acid catalyzed by PPP2-Fe including the binding processes of CO₂ and H₂(The shown values are Gibbs free energy in kJ/mol, calculation method: B3LYP/LANL2DZ/6-311+G^{*}; energy barrier for CO₂ insertion and H₂ activation are 30.3 and 87.6 kJ/mol respectively)

用PPP2-Fe为催化剂时, CO₂插入Fe—H键也很容易发生, 相应过程能垒只有28.4 kJ/mol (TS1_{PPP2-Fe})。

PPP1-Fe是我们研究的不同铁基催化剂中具有最低速控步骤能垒的一个, 其速控步骤能垒为357.8 kJ/mol, 催化活性与贵金属比较接近。同时, 这一能垒比我们研究的速控步骤能垒最高的PNP4-Fe降低了170.5 kJ/mol, 显示了配体良好的调控催化活性能力(表1)。以上结果为实验开发用于CO₂加氢制甲酸的高活性铁基催化剂提供了良好的借鉴和理论基础。

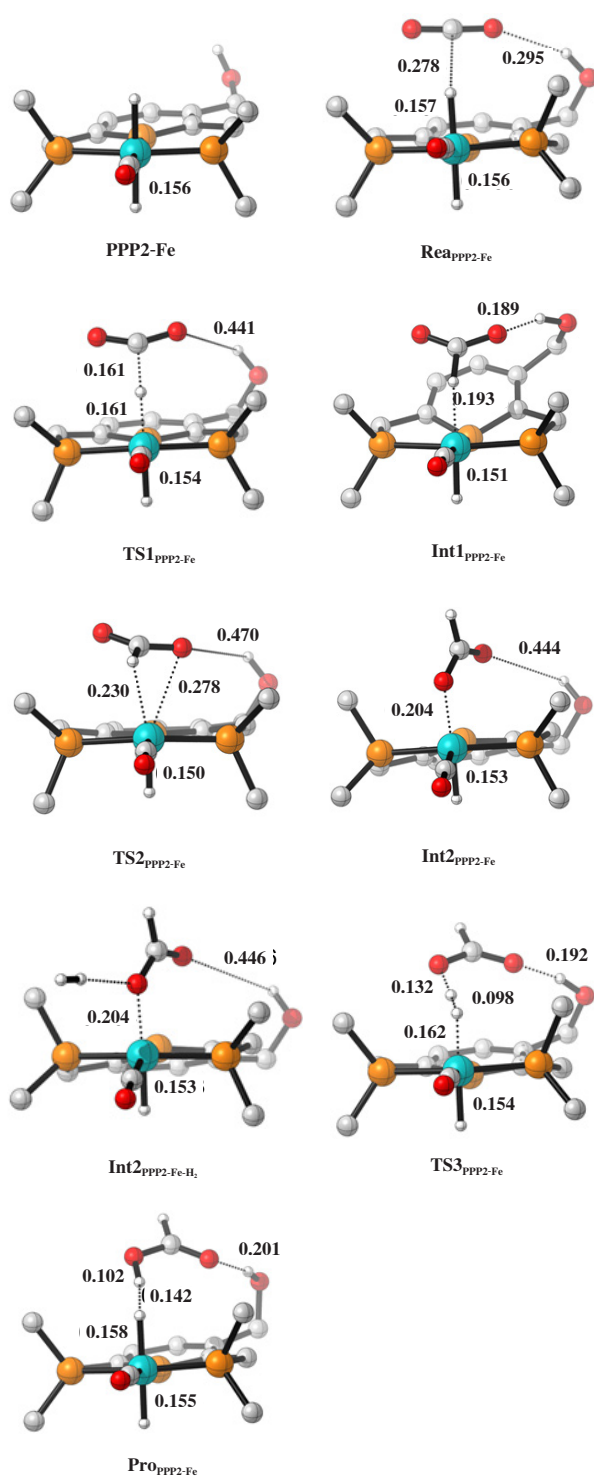


图9 含CO₂、H₂结合过程的PPP2-Fe催化的CO₂加氢制甲酸反应物、过渡态、中间体、产物的优化构型

Fig.9 The optimized structures of the reactant, transition states, and intermediates in the CO₂ hydrogenation to formic acid catalyzed by PPP2-Fe including the binding processes of CO₂ and H₂(The shown values are bond length in nm, calculation method: B3LYP/LANL2DZ/6-311+G^{*})

3 结论

为了探索用于CO₂加氢制甲酸的高活性铁基催化剂,采用理论计算的方法,系统研究了PNP-Ru以及12种不同PNP-Fe催化剂催化的CO₂加氢制甲酸过程。研究发现:CO₂加氢制甲酸包括H₂活化及CO₂插入金属氢键两个步骤,H₂活化是整个反应的速控步骤。铁基催化剂活性普遍低于Ru催化剂,但对PNP配体进行合理修饰可显著降低两种活性差异。PNP配体上的F原子取代会降低催化剂活性,而提供分子内氢键以及吡啶环上的P原子取代可增加催化剂活性。我们设计的铁基催化剂中,PPP1-Fe具有最高活性,其催化CO₂加氢制甲酸过程速控步骤能垒只有85.6 kJ/mol,这一活化能垒与贵金属的比较接近。我们研究的12种铁基催化剂速控步骤能垒范围为85.6~126.4 kJ/mol,显示了配体良好的调控催化活性能力。我们的研究结果可为高活性CO₂加氢制甲酸催化剂的开发提供理论指导和参考。

参考文献 :

- [1] a. Artz J, Muller T, Thenert K, et al. Sustainable conversion of carbon dioxide: An integrated review of catalysis and life cycle assessment[J]. *Chem Rev*, 2018, **118**(2): 434–504.
b. Liang Zhi-ming(梁志铭), Nie Xiao-wa(聂小娃), Guo Xin-wen(郭新闻), et al. DFT Insight into the effect of ni doping on hydrocarbons synthesis from CO₂ hydrogenation over Fe catalyst(镍掺杂对Fe催化剂上CO₂加氢制烃影响的理论计算研究)[J]. *J Mol Catal(China)* (分子催化), 2020, **34**(4): 293–303.
c. Pan Yin-yin(潘茵茵), Song Guang-jie(宋广杰), Xue Kuan-rong(薛宽荣), et al. The development of hydroformylation of alkenes and alkynes with syngas substitutes(非合成气法烯烃、炔烃氢甲酰化研究进展)[J]. *J Mol Catal(China)*(分子催化), 2021, **35**(2): 166–177.
- [2] a. Wang W H, Himeda Y, Muckerman J T, et al. CO₂ Hydrogenation to formate and methanol as an alternative to photo- and electrochemical CO₂ reduction [J]. *Chem Rev*, 2015, **115**(23): 12936–12973.
b. Aisha·Nulahong(艾沙·努拉洪), Fang Ya-ping(方亚平), Gao Xi-ran(高希然), et al. Effect of ZSM-5 zeolites with different grains on carbonylation of syngas(不同晶粒ZSM-5沸石分子筛对合成气羰基化反应性能的

- 影响)[J]. *J Mol Catal(China)*(分子催化), 2020, **34**(2): 105–115.
- [3] Hutschka F, Dedieu A, Eichberger M, et al. Mechanistic aspects of the rhodium-catalyzed hydrogenation of CO₂ to Formic acid a theoretical and kinetic study[J]. *J Am Chem Soc*, 1997, **119**(19): 4432–4443.
- [4] Zell T, Milstein D. Hydrogenation and dehydrogenation iron pincer catalysts capable of metal-ligand cooperation by aromatization/dearomatization[J]. *Acc Chem Res*, 2015, **48**(7): 1979–1994.
- [5] Yang X. Hydrogenation of carbon dioxide catalyzed by pnp pincer iridium, iron, and cobalt complexes: A computational design of base metal catalysts[J]. *ACS Catal*, 2011, **1**(8): 849–854.
- [6] Schmeier T J, Dobereiner G E, Crabtree R H, et al. Secondary coordination sphere interactions facilitate the insertion step in an Iridium(III) CO₂ reduction catalyst[J]. *J Am Chem Soc*, 2011, **133**(24): 9274–9277.
- [7] Hou C, Jiang J, Zhang S, et al. Hydrogenation of carbon dioxide using half-sandwich cobalt, rhodium, and iridium complexes: DFT study on the mechanism and metal effect[J]. *ACS Catal*, 2014, **4**(9): 2990–2997.
- [8] Kumar N, Camaioni D M, Dupuis M, et al. Mechanistic insights into hydride transfer for catalytic hydrogenation of CO₂ with cobalt complexes[J]. *Dalton Trans*, 2014, **13**: 11803–11806.
- [9] Filonenko G A, Hensen E J M, Pidko E A, et al. Mechanism of CO₂ hydrogenation to formates by homogeneous Ru-PNP pincer catalyst: From a theoretical description to performance optimization[J]. *Catal Sci Technol*, 2014, **4**: 3474–3485.
- [10] Rawat K S, Mahata A, Choudhuri I, et al. Catalytic hydrogenation of CO₂ by manganese complexes: Role of π-acceptor ligands[J]. *J Phy Chem C*, 2016, **120**(30): 16478–16488.
- [11] Sirijaraensre J, Limtrakul J. Hydrogenation of CO₂ to formic acid over a Cu-embedded graphene: A DFT study[J]. *Appl Surf Sci*, 2016, **364**: 241–248.
- [12] Ge H Y, Jing Y Y, Yang X Z, et al. Computational design of cobalt catalysts for hydrogenation of carbon dioxide and dehydrogenation of formic acid[J]. *Inorg Chem*, 2016, **55**(23): 12179–12184.
- [13] Mondal B, Neese F, Ye S, et al. Toward rational design of 3d transition metal catalysts for CO₂ hydrogenation based on insights into hydricity-controlled rate-determining steps[J]. *Inorg Chem*, 2016, **55**(11): 5438–5444.
- [14] Shi Xiao-yu(时晓羽), Li Hui-peng(李会鹏), Zhao Hua (赵华), et al. Solid-state Z-Scheme photocatalytic systems to splitting water and photo-reduce carbon dioxide (全固态Z-Scheme光催化材料应用于二氧化碳还原和光催化分解水研究进)[J]. *J Mol Catal(China)*(分子催化), 2019, **33**(4): 391–397.
- [15] Du Jie(杜杰), Zhang Ya-jing(张雅静), Zhang Yu(张宇), et al. Effect of SiO₂ promoter on performance of CuO-ZnO/HZSM-5 catalysts for synthesis of DME from CO₂ hydrogenation(SiO₂助剂对CuO-ZnO/HZSM-5催化CO₂加氢制DME性能的影响)[J]. *J Mol Catal(China)*(分子催化), 2016, **30**(4): 346–353.
- [16] Bertini F, Gorgas N, Stoger B, et al. Efficient and mild carbon dioxide hydrogenation to formate catalyzed by Fe(II) hydrido carbonyl complexes bearing 2,6-(diaminopyridyl) diphosphine pincer ligands[J]. *ACS Catal*, 2016, **6**(5): 2889–2893.
- [17] Tanaka R, Yamashita M, Nozaki K, et al. Catalytic hydrogenation of carbon dioxide using Ir(III)-pincer complexes[J]. *J Am Chem Soc*, 2009, **131**(40): 14168–14169.
- [18] Hull J F, Himeda Y, Wang W, et al. Reversible hydrogen storage using CO₂ and a proton-switchable iridium catalyst in aqueous media under mild temperatures and pressures[J]. *Nat Chem*, 2012, **4**: 383–388.
- [19] Anaby A, Feller M, Ben-David Y, et al. Bottom-up construction of a CO₂-based cycle for the photocarbonylation of benzene, promoted by a rhodium(I) pincer complex[J]. *J Am Chem Soc*, 2016, **138**(31): 9941–9950.
- [20] Qian Q, Zhang J, Cui M, et al. Synthesis of acetic acid via methanol hydrocarboxylation with CO₂ and H₂[J]. *Nat Commun*, 2016, **7**: 11481.
- [21] Li Z, Rayder T M, Luo L, et al. Aperture-opening encapsulation of a transition metal catalyst in a metal-organic framework for CO₂ hydrogenation[J]. *J Am Chem Soc*, 2018, **140**(26): 8082–8085.
- [22] Weilhard A, Qadir M I, Sans V, et al. Selective CO₂ hydrogenation to formic acid with multifunctional ionic liquids[J]. *ACS Catal*, 2018, **8**(3): 1628–1634.
- [23] Zhang X, Liu G, Meiwes-Broer K, et al. CO₂ activation and hydrogenation by PtHn- cluster anions[J]. *Angew Chem Int Ed*, 2016, **55**(33): 9644–9647.
- [24] Mori K, Sano T, Kobayashi H, et al. Surface engineering of a supported PdAg catalyst for hydrogenation of CO₂ to formic acid: Elucidating the active Pd atoms in alloy nanoparticles[J]. *J Am Chem Soc*, 2018, **140**(28): 8902–8909.

- [25] Liu G, Poths P, Zhang X, et al. CO₂ Hydrogenation to formate and formic acid by bimetallic palladium-copper hydride clusters[J]. *J Am Chem Soc*, 2020, **142**(17): 7930–7936.
- [26] Jiang Y, Blacque O, Fox T, et al. Catalytic CO₂ activation assisted by rhenium hydride/B(C₆F₅)₃ frustrated lewis pairs-metal hydrides functioning as FLP bases[J]. *J Am Chem Soc*, 2013, **135**(20): 7751–7760.
- [27] Zall C M, Linehan J C, Appel A M, et al. Triphosphine-ligated copper hydrides for CO₂ hydrogenation: Structure, reactivity, and thermodynamic studies[J]. *J Am Chem Soc*, 2016, **138**(31): 9968–9977.
- [28] Romero E A, Zhao T, Nakano R, et al. Tandem copper hydride-Lewis pair catalysed reduction of carbon dioxide into formate with dihydrogen[J]. *Nat Catal*, 2018, **1**: 743–747.
- [29] Kar S, Goeppert A, Kothandaraman J, et al. Manganese-catalyzed sequential hydrogenation of CO₂ to methanol via formamide[J]. *ACS Catal*, 2017, **7**(9): 6347–6351.
- [30] Dubey A, Nencini L, Fayzullin R R, et al. Bio-inspired Mn(I) complexes for the hydrogenation of CO₂ to formate and formamide[J]. *ACS Catal*, 2017, **7**(6): 3864–3868.
- [31] Langer R, Diskin-Posner Y, Leitus G, et al. Low-pressure hydrogenation of carbon dioxide catalyzed by an Iron pincer complex exhibiting Noble metal activity[J]. *Angew Chem Int Ed*, 2011, **50**(42): 9948–9952.
- [32] Curley J, Smith N, Bernskoetter W, et al. Understanding the reactivity and decomposition of a highly active Iron pincer catalyst for hydrogenation and dehydrogenation reactions[J]. *ACS Catal*, 2021, **11**(16): 10631–10646.
- [33] Lane E, Zhang Y, Hazari N, et al. Sequential hydrogenation of CO₂ to methanol using a pincer Iron catalyst[J]. *Organometallics*, 2019, **38**(15): 3084–3091.
- [34] Dai H, Li W, Krause J, et al. Experimental evidence of syn H-N-Fe-H configurational requirement for Iron-based bifunctional hydrogenation catalysts[J]. *Inorg Chem*, 2021, **60**(9): 6521–6535.
- [35] Jeletic M S, Mock M T, Appel A M, et al. A cobalt-based catalyst for the hydrogenation of CO₂ under ambient conditions[J]. *J Am Chem Soc*, 2013, **135**(31): 11533–11536.
- [36] Schneidewind J, Adam R, Baumann W, et al. Low-Temperature hydrogenation of carbon dioxide to methanol with a homogeneous cobalt catalyst[J]. *Angew Chem Int Ed*, 2017, **56**(7): 1890–1893.
- [37] Maia L B, Fonseca L, Moura I, et al. Reduction of carbon dioxide by a molybdenum-containing formate dehydrogenase: A kinetic and mechanistic study[J]. *J Am Chem Soc*, 2016, **138**(28): 8834–8846.
- [38] Zhao T, Hu X, Wu Y, et al. Hydrogenation of CO₂ to formate with H₂: Transition metal free catalyst based on a lewis pair[J]. *Angew Chem Int Ed*, 2019, **58**(3): 722–726.
- [39] Hu J, Liu J, Yao C, et al. Effective hydrogenation of CO₂ to formate catalyzed by ionic liquid modified acetate-Cu[J]. *Green Chem*, 2021, **23**: 951–956.
- [40] Schaub T, Paciello R. A process for the synthesis of formic acid by CO₂ hydrogenation: thermodynamic aspects and the role of CO[J]. *Angew Chem Int Ed*, 2011, **50**(32): 7278–7282.

Theoretical Calculation on the CO₂ Hydrogenation to Formic Acid and Design More Effective Iron Based Catalyst for this Process

LIU Cong¹, HU Xing-bang^{2*}

(1. Shandong GuoBang Pharmaceutical Co., Ltd., Weifang 261108, China; 2. School of Chemistry and Chemical Engineering, Nanjing University, Nanjing 210023, China)

Abstract: CO₂ hydrogenation is full of challenge because both H₂ and CO₂ are activated at the same time. This reaction also has 100% atomic economy. Most of the reported catalysts for CO₂ hydrogenation are based on noble metal. To find out more effective iron based catalysts for the CO₂ hydrogenation to formic acid, totally, the reaction processes catalyzed by 12 different PNP-Fe (PNP=2,6-bis(di-tert-butylphosphinomethyl)pyridine) compounds were investigated. The theoretic calculation results revealed that the CO₂ hydrogenation included two steps: H₂ activation and CO₂ inserting into the metal-hydride bond. The H₂ activation is the rate-determining step. It was found that P atom substitution on the pyridine ring could obviously reduce the H₂ activation barrier. Based on these findings, an effective Fe catalyst was designed, whose H₂ activation barrier was only 85.6 kJ/mol, being comparable to the data of precious metal catalyst. The H₂ activation barriers range from 85.6 to 126.4 kJ/mol for different Fe-based catalysts investigated here, indicating that the modification of ligand has great influence on the catalytic reactivity for the CO₂ hydrogenation.

Key words: CO₂; hydrogenation; formic acid; theoretical calculation; iron catalyst